24 September 1999

ELSEVIER

Chemical Physics Letters 311 (1999) 131–138

CHEMICAL PHYSICS LETTERS

www.elsevier.nl/locate/cplett

OH overtone spectra and intensities of pernitric acid

Lorien Fono [a], D.J. Donaldson [a,*], Robert J. Proos [b], Bryan R. Henry [b]

[a] *Scarborough College and Department of Chemistry, University of Toronto, Toronto, Ont. Canada M5S 1A1*
[b] *Department of Chemistry and Biochemistry, University of Guelph, Guelph, Ont. Canada N1G 2W1*

Received 14 June 1999; in final form 19 July 1999

Abstract

The integrated absorption intensities of the $3\nu_{OH}$ overtone transitions of the OH stretch of pernitric acid (HO_2NO_2) and nitric acid ($HONO_2$) were measured in concentrated sulfuric acid (H_2SO_4) solution. As well, oscillator strengths for the OH overtones of isolated HO_2NO_2 were calculated ab initio. Both results indicate that the OH overtones of HO_2NO_2 have larger oscillator strengths than the corresponding transitions in $HONO_2$ (1.3 ± 0.5 times greater in H_2SO_4 solution; about 2 times greater according to the ab initio calculations). Overtone-induced photodissociation of HO_2NO_2 could play a role in HO_x production at high solar zenith angles.

1. Introduction

Recently, measurements of HO_x (the sum of OH and HO_2) concentrations in the stratosphere have shown a very rapid onset of HO_x production at very high solar zenith angles (SZA), corresponding to the sun's being below the local horizon [1,2]. This is surprising, and was not predicted by atmospheric models, because in these models HO_x production is predominantly due to the reaction of $O(^1D)$ with water. The $O(^1D)$ species is produced predominantly by UV photolysis of ozone at $\lambda \leqslant 310$ nm, although there is a small quantum yield for its production at longer wavelengths [3]. At high SZAs, ultraviolet (UV) solar radiation is strongly attenuated by the long atmospheric pathlength through the ozone layer, so $O(^1D)$ production is severely reduced, reducing HO_x production to a minimum.

To account for at least a portion of the 'excess' HO_x production, Donaldson et al. [4] recently proposed a HO_x production mechanism which relies only on visible light, which is not strongly attenuated at high SZAs. In this mechanism, dubbed 'direct overtone photodissociation' (DOP), OH overtone transitions of trace species X–OH present in the stratosphere absorb visible radiation; if this light is sufficiently energetic to cause the X–O bond to cleave, then OH will be formed [5]. This 'overtone-mediated dissociation' mechanism has been studied for such molecules as $HONO_2$ (nitric acid) [6], HOOH (hydrogen peroxide) [7], HONO (nitrous acid) [8] and $HOOC(CH_3)_3$ (*t*-butyl peroxide) [9] in the context of measuring unimolecular reaction dynamics.

Incorporation of the DOP mechanism into radiative transfer models [4] suggested that of the known species with low R–OH bond strengths present in the stratosphere, H_2O_2, HNO_3, HONO and HO_2NO_2 (pernitric acid), OH production from DOP of HOOH would be insignificant, HNO_3 and HONO would

* Corresponding author. E-mail: jdonalds@chem.utoronto.ca

0009-2614/99/$ - see front matter
PII: S0009-2614(99)00858-1

play minor roles, but that HO_2NO_2, because of its low N–O bond energy (about 8760 cm^{-1}) [10], could be a significant source of HO_x at high SZAs.

These calculations required some knowledge of the absorption cross-sections for the OH overtone transitions. In the initial work, these were estimated, based on the values suggested by Crim [11]. Subsequently, we have performed a thorough study of the OH overtones in $HONO_2$ [12], combining measured and ab initio values to obtain cross-sections we estimate to be good to better than 25%. In the present work, we extend this study to HO_2NO_2. Ab initio values for the oscillator strengths are obtained and are found to be a factor of 2 larger than those for $HONO_2$. The integrated absorption cross-sections for the $3\nu_{OH}$ overtones of HO_2NO_2 and $HONO_2$ were measured in concentrated H_2SO_4 solution. The HO_2NO_2 result is a factor of 1.3 times larger than that of $HONO_2$.

2. Experimental

Solutions of various concentrations of $HONO_2$ and HO_2NO_2 in concentrated (95–98 wt%) H_2SO_4 were prepared volumetrically from stock concentrated solutions and cooled to room temperature prior to measurement. Commercial reagent-grade concentrated HNO_3 was used; the exact concentration of the stock solution was determined to be 79.3% (w/w) by titration against standardized KOH. The synthesis of HO_2NO_2 followed a modification of that given by Appleman and Gosztola [13]. In this procedure, 2.7 g $NaNO_2$ were dissolved in 11.8 ml 20% w/w HOOH and cooled to 0°C. Next, 7.8 ml of 20 wt.% HOOH were added to 0.75 ml of concentrated H_2SO_4, stirred, and cooled to -23°C in a carbon tetrachloride/dry-ice bath. The $NaNO_2$–peroxide solution was added to the acid–peroxide solution dropwise, using a syringe. After each of the first four additions of 2 ml, 0.5 ml of H_2SO_4 was added to the reaction mixture. This procedure gave a stock solution of approximately 1.75 M HO_2NO_2. Repeating this procedure with smaller amounts of $NaNO_2$ yielded lower concentrations of HO_2NO_2. The spectrum of the solution was measured immediately after preparation, to minimize decomposition of the HO_2NO_2.

Absorption spectra of $HONO_2$ and HO_2NO_2 were measured between 400 and 1100 nm in a commercial single-beam spectrometer, using cells of pathlength 5.00 or 10.00 cm. Background spectra were measured at the same time and subtracted from the sample spectra as detailed below. No absorbing species are present in these mixtures other than those of interest and H_2O. At the time of the visible scan of the HO_2NO_2 solutions, a UV spectrum from 250 to 400 nm was also measured in a 1.00 cm cell, with the reaction mixture diluted by a factor of 10 in order to get an absorbance between 0.2 and 0.8 in the 310–330 nm region.

Neither H_2O nor H_2SO_4 absorbs in this region of the spectrum. To determine the concentration of HO_2NO_2, the total absorbance of the reaction mixture at each of 310, 320 and 330 nm was measured. The total absorbance at each wavelength was assumed to be the sum of that due to absorption by HO_2NO_2 and by HOOH,

$$A_{\text{total}}/l = c_{H_2O_2}\varepsilon_{H_2O_2} + c_{HNO_4}\varepsilon_{HNO_4}. \quad (1)$$

Simultaneous solution of Eq. (1) at any two wavelengths yielded calculated concentrations of both HO_2NO_2 and the remaining, unreacted HOOH. The absorption coefficient of aqueous HOOH at the wavelengths used was measured here. The absorption coefficient of aqueous HO_2NO_2 reported by Jesson et al. [14] at these wavelengths was used. Errors in concentration were estimated to be the standard deviation of the three values arising from this procedure.

Visible spectra of H_2O in cold (~ 0°C) H_2SO_4 (and HOOH in H_2SO_4, in the case of HO_2NO_2) are unstructured in the $3\nu_{OH}$ and $4\nu_{OH}$ regions from 700 to 1100 nm. These background spectra were scaled and subtracted from the visible spectrum of the reaction mixture in the OH overtone regions. The scaling was varied (within reasonable stoichiometric limits) until the overtone peak had a flat baseline in the subtracted spectrum. The integrated absorbance of each overtone band was determined at a number of concentrations; a plot of A/l versus concentration yields a straight line with the integrated cross-section as slope. The errors in the integrated absorbance arise primarily from the range of scaling which could be applied to the background spectrum

and still result in a physically reasonable subtracted spectrum.

3. Calculations

The ab initio determination of the overtone oscillator strengths was performed in the same manner as previously reported for $HONO_2$ [12]. This method has proved very successful in reproducing experimental intensities for a number of molecules, over a range of six orders of magnitude in intensity [12,15–21]. Intensities for C–H overtones are reproduced to better than a factor of two; calculated O–H overtone intensities are within 25% of measured values. The oscillator strengths, $f_{g\to e}$, of vibrational overtone transitions from $|g\rangle$ to $|e\rangle$ are given by [22]:

$$f_{g\to e} = 4.70165\times 10^{-7}\ (\mathrm{cm\,D^{-2}})\ \nu_{eg}|\boldsymbol{\mu}_{eg}|^2, \quad (2)$$

where ν_{eg} gives the transition frequency in cm^{-1} and $\boldsymbol{\mu}_{eg}$ represents the transition dipole moment matrix element, $\langle e|\boldsymbol{\mu}|g\rangle$ in debye. The oscillator strength can be shown to be related to the integrated absorption cross-section, $\sigma(\nu)$, by [22]:

$$f = 1.1296\times 10^{12}\int \sigma(\nu)\,\mathrm{d}\nu .$$

In order to calculate the oscillator strength of an overtone transition, the transition energy and the dipole moment function are required. The wavefunctions describing the OH stretch are approximated as the eigenfunctions of a Morse oscillator whose transition energies to level υ from the ground vibrational state, $\nu_{\upsilon\leftarrow 0}$, are given by:

$$\nu_{\upsilon\leftarrow 0} = \upsilon\omega - (\upsilon^2+\upsilon)\,\omega\chi , \quad (3)$$

where ω and $\omega\chi$ represent the vibrational frequency and anharmonicity constants (in cm^{-1}), respectively. These parameters are not known experimentally for HO_2NO_2, so were calculated here. For a Morse oscillator, ω and $\omega\chi$ are related to the bond dissociation energy by:

$$D_e = \omega^2/4\omega\chi . \quad (4)$$

The dissociation energy was calculated ab initio, using the GAUSSIAN 98 suite of programs [23]. In conjunction with the reported value of the fundamental frequency (3540 cm^{-1}) [24], values for ω and $\omega\chi$ could then be determined.

In these calculations, the dipole moment function is expressed as a seventh-order Taylor series expansion in the internal O–H bond length co-ordinate, q, expanded about the equilibrium position:

$$\boldsymbol{\mu}(q) = \Sigma\,\boldsymbol{\mu}_i q^i , \quad (5)$$

where the coefficients $\boldsymbol{\mu}_i$ are given by:

$$\mu_i = \frac{1}{i!}\frac{\partial^i\mu}{\partial R^i}\Big|_e . \quad (6)$$

The equilibrium O–H bond distance was determined by performing a geometry optimization at the QCISD/6-31 + G(d,p) level. The coefficients given in Eq. (6) were obtained by changing the H–O bond length by ± 0.4 Å in increments of 0.1 Å and calculating the dipole moment at each position using ab-initio quantum calculations. Numerical analysis was used to give the coefficients [6] which were used to construct the dipole moment function [5]. This, the Morse wavefunctions and the transition energies given by [3], were used in Eq. (2) to calculate the oscillator strengths.

4. Results and discussion

4.1. Experimental

Overtone spectra are observed in the $3\nu_{OH}$ region for both HNO_3 and HO_2NO_2 and in the $4\nu_{OH}$ region for HNO_3. The spectra of $HONO_2$ and HO_2NO_2 in the $3\nu_{OH}$ region are displayed in Figs. 1 and 2, respectively. In both molecules, at low concentrations a double peak is observed in the $3\nu_{OH}$ spectra, with maxima at 980 and 1015 nm in $HONO_2$ and at 970 and 995 nm in HO_2NO_2. In the $HONO_2$ spectrum, the bands lie very close to the measured gas-phase absorption [12]. No overtone spectra have been reported previously for HO_2NO_2. The somewhat broader red component of each double peak becomes relatively less intense as the concentration is increased. This effect is shown in Fig. 2 for HO_2NO_2. We interpret the double peaks as being due to a combination of solvation and hydrogen bonding/complex formation effects. Since the higher-energy component of the double peak becomes more pronounced with increasing concentration, we assign it to the complexed species; the lower-energy compo-

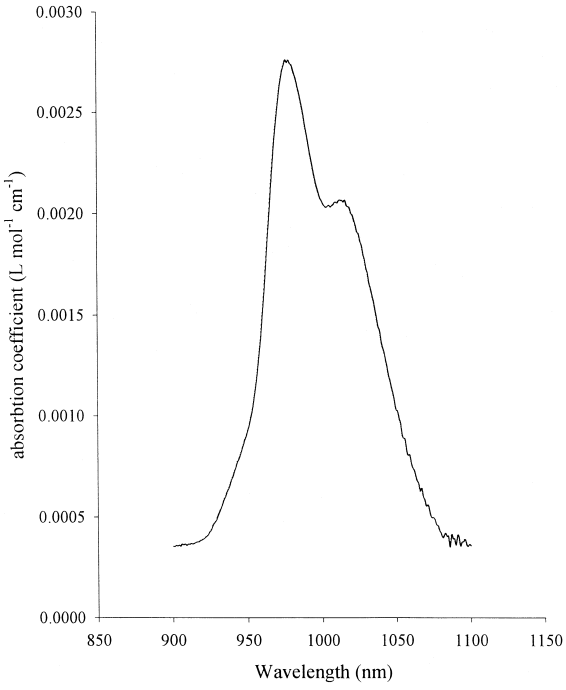

Fig. 1. Overtone absorption spectrum in the 3 ν_{OH} region of 3.9 M $HONO_2$ in concentrated H_2SO_4 solution.

nent is assigned to the uncomplexed (but solvated) species. We take the sum of the total integrated intensity of both peaks for comparison to the integrated absorption cross-section in the gas phase.

To ensure that the feature in the $3\nu_{OH}$ spectral region in the HO_2NO_2 sample is really due to HO_2NO_2, we performed several checks. A Raman spectrum of a concentrated sample was measured and showed peaks corresponding to those given by Appleman and Gosztola [13], in which the spectrum was measured in perchloric acid solvent. As well, to ensure that the overtone is not due to HONO, a sample was prepared as above, but without addition of H_2O_2. HONO may be synthesized from the reaction of $NaNO_2$ in (dilute) H_2SO_4 [25]. A very weak peak is observed at 950 nm under these conditions; no such feature is measured in either the HNO_3 or HO_2NO_2 spectra. As well, the spectra of H_2O_2 and H_2O were each measured in dilute (2.6 M) H_2SO_4; these showed absorption features due to their $3\nu_{OH}$ bands at 1020 and 980 nm, respectively. We conclude that the absorption features shown in Fig. 2 are assignable to the $3\nu_{OH}$ overtone of HO_2NO_2.

Plots of the integrated absorbance divided by the cell pathlength of the $3\nu_{OH}$ bands versus concentration, as given by Eq. (1), are shown in Fig. 3 for HNO_3 and in Fig. 4 for HO_2NO_2. These plots are linear, with no indication of breaks or discontinuities, suggesting that taking the sum of the integrated absorbances of the two peaks which appear at lower concentrations is a valid approach. The slopes of these plots yield the integrated absorption cross-sections, which are presented in Table 1. The integrated absorption cross-sections obtained for the $3\nu_{OH}$ and $4\nu_{OH}$ transitions of $HONO_2$ are factors of 3.6 and 6.1 less than the corresponding values in the gas phase, 2.63×10^{-20} and 2.37×10^{-21} cm^2 molecule^{-1} cm^{-1}, respectively [12].

Clearly, because of solvent effects on the overtone intensities, the solution-phase results should not be directly compared with gas-phase values. However, the qualitatively similar nature of the overtone spectra (double peaks at lower concentrations; single peaks at higher concentrations) suggests that solva-

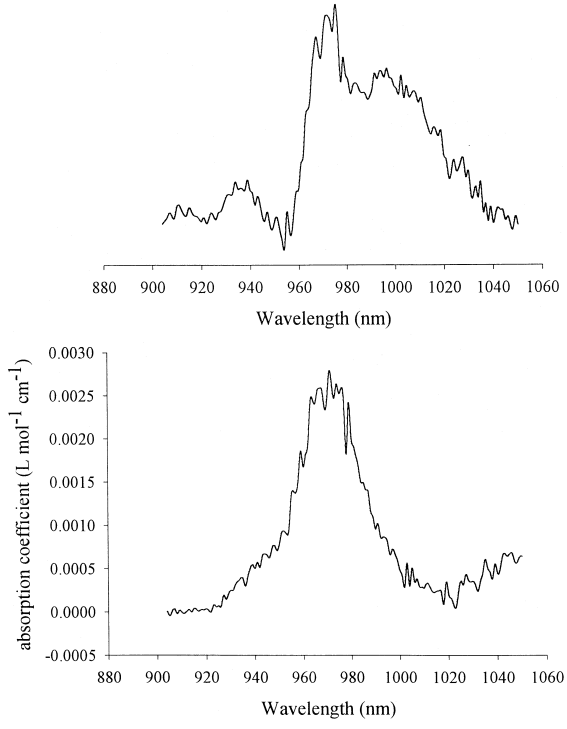

Fig. 2. Overtone absorption spectrum in the 3 ν_{OH} region of HO_2NO_2 in concentrated H_2SO_4 solution at two different concentrations. Upper panel: 0.5 M; lower panel: 1.2 M.

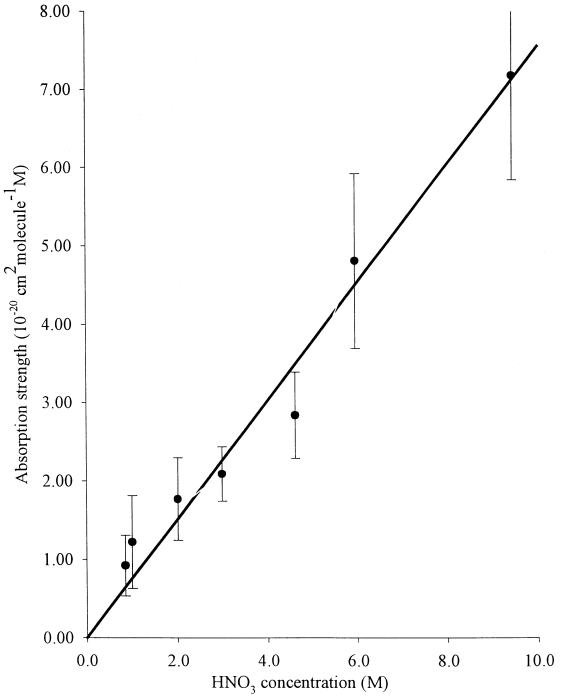

Fig. 3. Beer's law plot of the integrated absorbance divided by the cell pathlength of the $HONO_2$ 3 ν_{OH} band as a function of concentration in H_2SO_4. The units have been converted from the conventional solution-phase units in order to obtain integrated cross-sections in cm^2 molecule^{-1} cm^{-1}, for comparison to the gas-phase values. The slope of this plot is the integrated absorption cross-section. It is $(7.2 \pm 1.1) \times 10^{-21}$ cm^2 molecule^{-1}.

tion affects the overtone intensities of $HONO_2$ and HO_2NO_2 similarly. If this is the case, the ratio of the observed integrated absorption cross-sections of HO_2NO_2 to HNO_3 may be used to scale the measured gas-phase intensity of HNO_3 to obtain the gas-phase intensity of HO_2NO_2. This procedure yields a scaling of 1.3 ± 0.5 for the intensity ratio of the $3\nu_{OH}$ band of HO_2NO_2 acid relative to the same band of $HONO_2$.

4.2. Calculations

The O–H dissociation energies of HO_2NO_2, $HONO_2$, H_2O and HOOH were calculated using two basis sets (6-31G(d) and 6-31 + G(d,p)) at the QCISD and QCISD(T) levels. The results are shown in Table 2. These values and the known fundamental frequencies for the OH stretch in these molecules were used in conjunction with Eqs. (3) and (4) to predict the vibrational frequency and anharmonicity constants. The predicted and experimental values of these parameters are given in Table 3. Clearly, the best agreement with experiment is shown by the QCISD/6-31 + G(d,p) results, which lie within 0.2% of experiment for the vibrational frequency constant and 4.5% for the anharmonicity constant.

At this level of calculation, the calculated D_e for $HONO_2$ is 4.03% higher than that obtained using Eq. (4) and the experimental values of ω and $\omega\chi$. Similarly, the ab initio values of D_e calculated for H_2O and HOOH are overestimated by 2.04% and 3.19%, respectively. Taking an average 'overcalculation' of D_e of 3.09%, we may correct the ab initio values and use these corrected values to predict vibrational parameters. These are displayed in Table 4 for all four molecules. Using the corrected parameters for HNO_3 yields predicted (experimental) [12]

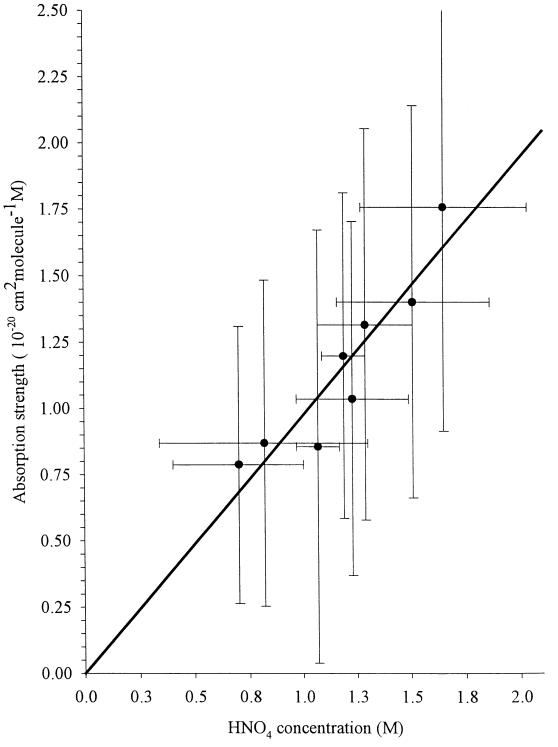

Fig. 4. Beer's law plot of the integrated absorbance of the HO_2NO_2 3 ν_{OH} band as a function of concentration in H_2SO_4. The slope of the best-fit line through the data points is $(9.7 \pm 2.5) \times 10^{-21}$ cm^2 molecule^{-1}.

Table 1
Integrated absorption cross-sections[a]

Species	$3\nu_{OH}$		$4\nu_{OH}$	
	gas[b]	solution	gas[b]	solution
HNO_3	$(2.63 \pm 0.26) \times 10^{-20}$	$(7.5 \pm 1.1) \times 10^{-21}$	$(2.37 \pm 0.24) \times 10^{-21}$	$(3.9 \pm 1.1) \times 10^{-22}$
HO_2NO_2		$(9.7 \pm 2.5) \times 10^{-21}$		

[a] Integrated intensities in cm^2 $molecule^{-1}$ cm^{-1}.
[b] From Ref. [12].

Table 2
Calculated H–O bond energies[a]

Theory	HO_2NO_2	$HONO_2$	HOH	HOOH
QCISD/6-31G(d)	37622	54125	42872	38266
QCISD/6-31 + G(d,p)	40920	45241	46550	41346
QCISD(T)/6-31G(d)	28806	46055	35977	28214

[a] Energies in cm^{-1}.

transition energies in (cm^{-1}) to $v = 3$–6 of 10180 (10173); 13261 (13245); 16185 (16165); 18952 (18940) respectively.

Table 5 presents the transition frequencies and oscillator strengths calculated for HO_2NO_2. The first column shows the results using the vibrational parameters and transition energies as calculated above. We also performed two other types of scaling to obtain the vibrational parameters. In the first, the ratio of the experimental values of the dimensionless anharmonicity $C\,(=\omega/2\,\omega\chi)$ of HOOH $(C = 21.15)$ to that of H_2O $(C = 23.58)$ was used to scale that for

Table 3
Morse parameters for OH stretches

Theory		HO_2NO_2	$HONO_2$	HOH	HOOH
QCISD/6-31G(d)	ω	3724	3675	3881	3799
	$\omega\chi$	92.2	62.4	87.8	94.3
QCISD/6-31 + G(d,p)	ω	3708	3701	3866	3783
	$\omega\chi$	84.0	75.7	80.3	86.5
QCISD(T)/6-31G(d)	ω	3789	3698	3919	3876
	$\omega\chi$	125	74.2	107	133
Experiment	ω		3707 [b]	3869.6[c]	3789.4[d]
	$\omega\chi$		79	82.06	89.6

[a] Energies in cm^{-1}.
[b] From Ref. [12].
[c] From Ref. [19].
[d] From Ref. [27].

Table 4
Corrected morse parameters

	HO_2NO_2	$HONO_2$	HOH	HOOH
D_e (cm^{-1})	39693	43885	45155	40107
ω (cm^{-1})	3714	3706	3871	3789
$\omega\chi$ (cm^{-1})	86.9	78.3	83.0	89.5

Table 5
Predicted peak positions and oscillator strengths for HO_2NO_2

V	Ab initio		C-scaling		D_e-scaling	
	ν (cm^{-1})	f	ν (cm^{-1})	f	ν (cm^{-1})	f
3	10099	5.66×10^{-8}	10090	5.81×10^{-8}	10076	6.06×10^{-8}
4	13118	4.02×10^{-9}	13100	4.21×10^{-9}	13072	4.52×10^{-9}
5	15963	4.86×10^{-10}	15934	5.14×10^{-10}	15887	5.63×10^{-10}
6	18635	7.13×10^{-11}	18591	7.66×10^{-11}	18521	8.60×10^{-11}
7	21132	1.15×10^{-11}	21071	1.26×10^{-11}	20973	1.46×10^{-11}

$HONO_2$ ($C = 23.46$) to yield a predicted value for HO_2NO_2 ($C = 21.04$). Using this parameter with the experimental fundamental frequency gives predicted values of ω and $\omega\chi$; the corresponding transition energies and oscillator strength are shown in the second column of Table 5. The second alternative scaling method was to scale the O–H dissociation energy of H_2O_2 by that of H_2O, then to use that factor to predict the D_e for the OH bond of HO_2NO_2 from that of $HONO_2$. This predicted D_e is then used with the experimental value for the vibrational fundamental to obtain ω and $\omega\chi$. The final column of Table 5 shows the results of that approach for the transition energies and oscillator strengths.

To compare these results with experiment, we take the ratio of the calculated HO_2NO_2 oscillator strengths divided by the corresponding values calculated [12] for $HONO_2$. The ab initio values of the oscillator strengths for the $3\nu_{OH}$ and $4\nu_{OH}$ transitions in $HONO_2$, calculated as outlined above but using experimental transition frequencies, are 2.78×10^{-8} and 2.14×10^{-9}, respectively [12]. These values differ on average by only 15% from the experimentally measured oscillator strengths. The ratios of the calculated oscillator strengths for HO_2NO_2 to $HONO_2$ range from 2.04 to 2.18 for the $3\nu_{OH}$ transition, and 1.88–2.11 for the $4\nu_{OH}$ transition, depending on which approach is used to calculate the HO_2NO_2 vibrational parameters.

Both experiment and theory indicate that the absorption cross-sections to the OH overtones in HO_2NO_2 are larger than the corresponding cross-sections in $HONO_2$. Every method used to calculate the oscillator strength yields this qualitative result; the quantitative agreement among the different approaches is quite good as well, suggesting that this result is robust. Given the uncertainties surrounding gas-solution changes in overtone absorption strengths, and the good agreement of theory and experiment in the case of $HONO_2$, we feel that the ab initio values are likely to be closer to the gas-phase oscillator strengths for HO_2NO_2 than those obtained from the H_2SO_4 solution experiments.

5. Conclusions

Both the ab initio results and the spectra measured in H_2SO_4 indicate that the OH overtone transitions in HO_2NO_2 have larger oscillator strengths than the corresponding transitions of $HONO_2$. We conclude that the oscillator strengths for OH overtones in HO_2NO_2 are probably at least 1.5 times larger than the corresponding values for $HONO_2$. This result suggests that DOP of HO_2NO_2 at high SZAs could be significant [26].

Acknowledgements

The financial support of NSERC is gratefully acknowledged. We thank Dr. A.F. Tuck and Prof. V. Vaida for many productive discussions.

References

[1] P.O. Wennberg, R.C. Cohen, R.M. Stimpfle, J.P. Koplow, J.G. Anderson, R.J. Salawitch, D.W. Fahey, E.L. Woodbridge, E.R. Keim, R.S. Gao, C.R. Webster, R.D. May, D.W. Toohey, L.M. Avallone, M.H. Proffitt, M. Loewenstein, J.R. Podolske, K.R. Chan, S.C. Wofsy, Science 266 (1994) 398.
[2] P.O. Wennberg, R.J. Salawitch, D.J. Donaldson, T.F. Hanisco, E.J. Lanzendorf, K.K. Perkins, S.A. Lloyd, V. Vaida, R.S. Gao, E.J. Hintsa, R.C. Cohen, W.H. Schartz,

T.L. Kusterer, D.E. Anderson, Geophys. Res. Lett. 26 (1999) 1373.
[3] A.R. Ravishankara, G. Hancock, M. Kawasaki, Y. Matsumi, Science 280 (1998) 60, and references therein.
[4] D.J. Donaldson, G.J. Frost, K.H. Rosenlof, A.F. Tuck, V. Vaida, Geophys. Res. Lett. 24 (1997) 2651.
[5] F.F. Crim, Annu. Rev. Phys. Chem. 44 (1993) 397.
[6] A. Sinha, R.L. Vander Wal, F.F. Crim, J. Chem. Phys. 92 (1990) 401.
[7] L.J. Butler, T.M. Ticich, M.D. Likar, F.F. Crim, J. Chem. Phys. 85 (1986) 2331.
[8] S.M. Holland, R.J. Strickland, M.N.R. Ashfold, D.A. Newnham, I.M. Mills, J. Chem. Soc. Faraday Trans. 87 (1991) 3461.
[9] M.D. Likar, J.E. Baggott, F.F. Crim, J. Chem. Phys. 90 (1989) 6266.
[10] R. Atkinson, D.L. Baulch, R.A. Cox, R.F. Hampson Jr., J.A. Kerr, M.J. Rossi, J. Troe, J. Phys. Chem. Ref. Data 26 (1997) 521.
[11] F.F. Crim, Annu. Rev. Phys. Chem. 35 (1984) 657.
[12] D.J. Donaldson, J. Orlando, G. Tyndall, R. Proos, B. Henry, V. Vaida, J. Phys. Chem. A 102 (1998) 5171.
[13] E.H. Appleman, D.J. Gosztola, Inorg. Chem. 34 (1995) 787.
[14] J.P. Jesson, L.C. Glasgow, D.L. Filkin, C. Miller, Geophys. Res. Lett. 4 (1977) 513.
[15] D.M. Turnbull, H.G. Kjaergaard, B.R. Henry, Chem. Phys. 195 (1995) 129.
[16] H.G. Kjaergaard, D.M. Turnbull, B.R. Henry, J. Chem. Phys. 99 (1993) 9438.
[17] H.G. Kjaergaard, B.R. Henry, H. Wei, S. Lefebvre, T. Carrington Jr., O.S. Mortensen, M.L. Sage, J. Chem. Phys. 100 (1994) 6228.
[18] H.G. Kjaergaard, B.R. Henry, A.W. Tarr, J. Chem. Phys. 94 (1991) 5844.
[19] H.G. Kjaergaard, B.R. Henry, Mol. Phys. 83 (1994) 1099.
[20] H.G. Kjaergaard, R.J. Proos, D.M. Turnbull, B.R. Henry, J. Phys. Chem. 100 (1996) 19273.
[21] H.G. Kjaergaard, C.D. Daub, B.R. Henry, Mol. Phys. 90 (1997) 201.
[22] P.W. Atkins, Molecular Quantum Mechanics, 2nd edn., Oxford University Press, Oxford, 1983.
[23] M.J. Frisch, G.W. Trucks, H.B. Schlegel, G.E. Scuseria, M.A. Robb, J.R. Cheeseman, V.G. Zakrzewski, J.A. Montgomery, Jr., R.E. Stratmann, J.C. Burant, S. Dapprich, J.M. Millam, A.D. Daniels, K.N. Kudin, M.C. Strain, O. Farkas, J. Tomasi, V. Barone, M. Cossi, R. Cammi, B. Mennucci, C. Pomelli, C. Adamo, S. Clifford, J. Ochterski, G.A. Petersson, P.Y. Ayala, Q. Cui, K. Morokuma, D.K. Malick, A.D. Rabuck, K. Raghavachari, J.B. Foresman, J. Cioslowski, J.V. Ortiz, B.B. Stefanov, G. Liu, A. Liashenko, P. Piskorz, I. Komaromi, R. Gomperts, R.L. Martin, D.J. Fox, T. Keith, M.A. Al-Laham, C.Y. Peng, A. Nanayakkara, C. Gonzalez, M. Challacombe, P.M.W. Gill, B. Johnson, W. Chen, M.W. Wong, J.L. Andres, C. Gonzalez, M. Head-Gordon, E.S. Replogle, J.A. Pople, GAUSSIAN98, Revision A.5, Gaussian, Pittsburgh, PA, 1998.
[24] H. Niki, P.D. Maker, C.M. Savage, L.P. Breitenbach, Chem. Phys. Lett. 45 (1977) 564.
[25] A. Bongartz, J. Kames, F. Welter, U. Schurath, J. Phys. Chem. 95 (1991) 1076.
[26] D.J. Donaldson, A.F. Tuck, V. Vaida, submitted to Physics and Chemistry of the Earth, May 1999.
[27] H.G. Kjaergaard, J.D. Goddard, B.R. Henry, J. Chem. Phys. 95 (1991) 5556.